Diffusion theory of multidimensional activated rate processes: The role of anisotropy[a)]

M. M. Klosek-Dygas
Department of Mathematics, University of California, Davis, California 95616

B. M. Hoffman
Department of Chemistry, Northwestern University, Evanston, Illinois 60208

B. J. Matkowsky
Department of Engineering Sciences and Applied Mathematics, Northwestern University, Evanston, Illinois 60208

A. Nitzan
Department of Chemistry, Tel Aviv University, Tel Aviv, Israel

M. A. Ratner
Department of Chemistry, Northwestern University, Evanston, Illinois 60208

Z. Schuss
Department of Mathematics, Tel Aviv University, Tel Aviv, Israel

(Received 20 June 1988; accepted 5 October 1988)

We consider an anisotropic multidimensional barrier crossing problem, in the Smoluchowski (diffusion) limit. The anisotropy arises from either or both the shape of the potential energy surface and anisotropic diffusion. In such situations, the separatrix, which separates reactant and product regions of attraction, does not coincide with the ridge of the potential surface, which separates reactant and product wells, thus giving rise to a complicated time evolution. In the asymptotically long time limit, the time evolution is governed by crossing the separatrix and is exponential with a rate which may be obtained as a generalization of Kramers' theory to the anisotropic situation. In contrast, in long, though not asymptotically long times, the time evolution is dominated by repeated crossings of the ridge, and is nonexponential. Such nonexponential time evolution has been observed in many biochemical reactions, where many degrees of freedom and anisotropic diffusion processes lead to complicated dynamical behavior. Our model provides a simple prototype of such situations.

I. INTRODUCTION

The diffusion theory of activated rate processes, first introduced by Kramers[1] as one limit of his theory of chemical reaction rates, has been traditionally applied to models characterized by (i) one reaction coordinate defined by minimizing the potential energy along the reaction path and (ii) a potential barrier height larger than the thermal energy $k_B T$. A now standard treatment based on the Smoluchowski (diffusion) limit of the Fokker–Planck equation for this model yields[2]

$$k = \frac{1}{2\pi} \frac{\Pi_j \omega_j^W}{\gamma \Pi_{nr} \omega_{nr}^B} \omega_r^B e^{-\Delta V/k_B T}, \tag{1.1}$$

where ΔV is the height of the potential barrier, T the temperature, k_B Boltzmann's constant, γ is the friction coefficient, ω_r^B and ω_{nr}^B are the frequencies associated with the reactive and nonreactive coordinates at the barrier (saddle point), and ω_j^W are the normal mode frequencies associated with the reactant well. The products Π_{nr} and Π_j are taken over all the corresponding modes.

Equation (1.1) is a very useful tool for describing and analyzing activated rate processes in the overdamped (diffusion) limit. The reason that the reaction can generally be described in terms of a single linear reaction path, is that in the diffusion limit the system is essentially in equilibrium everywhere but in the immediate vicinity of the saddle point. The dynamics may therefore be evaluated by considering the linearized potential surface about this point. There have been claims[3] that reaction path curvature may lead to nontrivial corrections to Eq. (1.1), however some of us have recently shown[4] that such corrections result from the anharmonicity of the potential surface and from the presence of a small window frequency (small ω_{nr}^B) at the saddle, and that reaction path curvature is irrelevant in the diffusion limit.

Experimentally, the validity of Eq. (1.1) has been verified in many situations. There are cases however where the observed kinetics does not follow a simple rate equation even when the assumptions that lead to Eq. (1.1) seem to be valid. A notable example is the low temperature kinetics of ligand binding to heme protein.[5] In a typical experiment the heme–ligand complex is pulse irradiated in order to flash off the ligand, and the recombination kinetics is followed spectroscopically on a microsecond time scale. It is believed that the

[a)] This research was supported in part by the U.S.–Israel Binational Science Foundation, The Israel Academy of Sciences and Humanities, DOE Grant DEFG-02-87ER25027, NSF Grant DMS 8703011, the Coal Chemistry Program of GRI and NIH Grant PCM 8350218.

 0021-9606/89/021141-08$02.10

observed recombination is a process in which the ligand moves from the periphery of the protein into the heme pocket.[5] The observed nonexponential kinetics in this and other structural reorganization processes in large biomolecular systems may be explained by models which assume the existence of intermediate locally stable states, implying that the observed reaction is dominated by several barrier crossing processes. The observed kinetics is however not easily resolved into a sum of just a few exponentials. Sometimes successful fits to power law time dependence suggest that a continuous spectrum of relaxation times exists. Another important experimental observation is that the time evolution becomes more exponential-like at higher temperatures. This suggests that the nonexponential time evolution is related to the multitude of degrees of freedom associated with the large molecule. When the temperature is sufficiently high, the rate at which the molecule explores the configuration subspace associated with the reactant conformations, is relatively fast and the observed rate is dominated by the slower crossing at the saddle point. At lower temperatures, other relaxation times may fall within the experimental time scale and even though the long time kinetics is still dominated by the slowest barrier crossing process, shorter time nonexponential kinetics may be observed.

In this paper we investigate a simple two-dimensional model which has these properties and which may be used as a prototype for such processes. The model consists of a diffusional barrier crossing in two dimensions (Fig. 1) where anisotropy in both the shape of the potential surface and in the friction coefficients, and consequently also in the diffusion tensor, is taken into account. For simplicity we consider the situation in which the principal axes of the reactant and product wells, as well as the principal axes of the diffusion tensor, are parallel. In our analysis, we employ a coordinate system which is parallel to these principal axes. We shall see that in this situation a one-dimensional reaction coordinate defined near the saddle point (taken to be the origin) is not sufficient to describe the time evolution of the system. We shall also show that such anisotropies may lead to nonexponential transient evolution, that may correspond to relevant experimental times. In Fig. 1 we show two examples for the systems considered here. Figure 1(a) is a schematic representation of the ligand–heme protein potential surface.[6] Figure 1(b) is a plot of the potential corresponding to the lower eigenvalue of the 2×2 vibronic coupling potential matrix

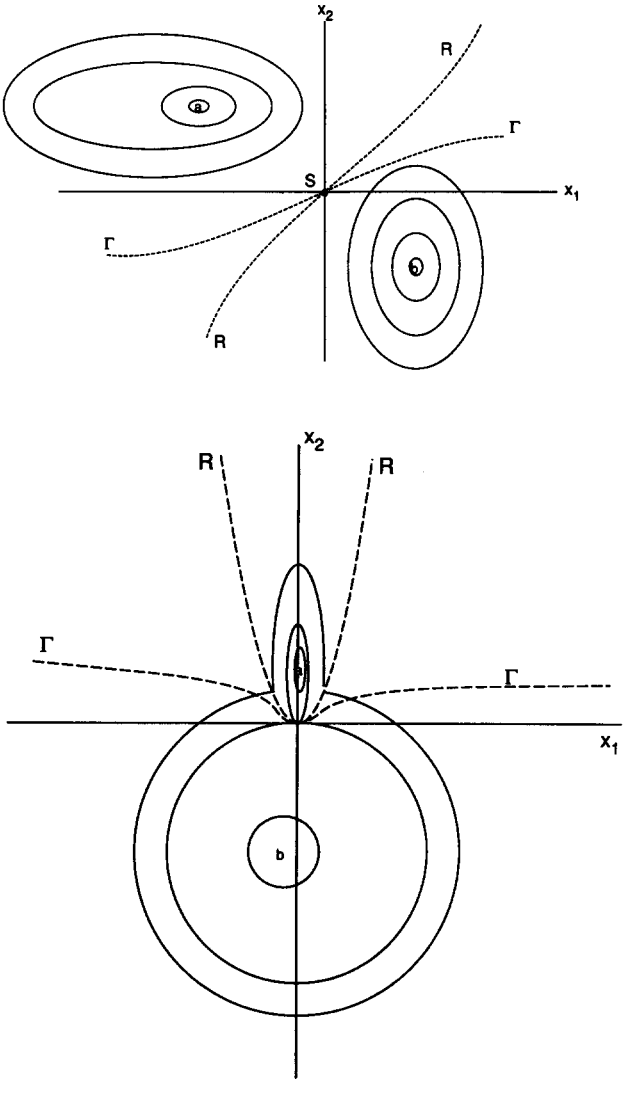

FIG. 1. (a) A schematic sketch of the potential surface for the ligand protein rebinding reaction. R denotes the ridge, Γ the separatrix, and S the saddle point. The stable reactant and product configurations are denoted by a and b, respectively. Note that the shapes and orientations of R and Γ are schematic and other possibilities exist as discussed in the text. (b) A plot of the potential corresponding to the lower eigenvalue of the 2×2 vibronic coupling matrix (1.2). The parameters used are $k_1=20$, $k_2=1$, $l_1=l_2=1$, $\lambda_1=0.1$, $\lambda_2=0.262$, $\mu_1=1$, $\mu_2=2.618$, $\Delta=0.1$, and $t=0.1$. The ratio of the diffusion coefficients is $\delta=0.1$. The ridge and separatrix shown in the figure have been calculated for this choice of parameters. Note that unlike the situation in the schematic picture (a), R and Γ touch (at the saddle point) but do not cross each other.

$$V(x_1,x_2)=\begin{pmatrix} \frac{1}{2}k_1x_1^2+\frac{1}{2}l_1x_2^2+\lambda_1x_1+\mu_1x_2 & t \\ t & \frac{1}{2}k_2x_1^2+\frac{1}{2}l_2x_2^2-\lambda_2x_1-\mu_2x_2+\Delta \end{pmatrix} \tag{1.2}$$

with parameter values given in the figure caption.

A similar point concerning the inadequacy of a one-dimensional treatment of the diffusion along the reaction coordinate has been previously made by Agmon and Hopfield[6] who studied a diffusion equation with a reactive sink

$$\frac{\partial\rho(x,t)}{\partial t}=D\left[\frac{\partial^2\rho}{\partial x^2}+\frac{1}{k_BT}\frac{\partial}{\partial x}\left(\rho\frac{\partial V}{\partial x}\right)\right]-k(x)\rho. \tag{1.3}$$

The origin of the sink term $k(x)\rho$ can be, for example, quantum mechanical electron tunneling, in which case Eq. (1.2) may be used to describe diffusion control of electron transfer processes. In the case of CO binding, discussed in Ref. 6, the sink was taken to correspond to irreversible binding of CO when the system crosses the ridge, separating reactant (unbound CO) and product (bound CO) regions of the poten-

tial surface. Equation (1.2) is indeed a useful tool for describing processes in which the reactive step [corresponding to the last term of Eq. (1.3)] is not diffusion controlled. For processes in which the process modeled by $k(x)$, originates from a diffusion along another coordinate, it is not clear that Eq. (1.3) is valid. In this case, which seems to describe processes such as ligand–heme protein binding, the full multidimensional diffusion equation has to be investigated, as is done below. We do however retain an essential point of the Agmon–Hopfield treatment, namely that the nonequivalence between the two directions is expressed in terms of anisotropies in both the potential surface and the diffusion tensor as discussed above. We remark that our treatment is classical. A quantum treatment of a related model of electron transfer was considered in Ref. 7.

The existence of nonisotropic diffusion in our model is associated with the fact that different degrees of freedom (e.g., different motions and/or motions of different atomic groups) in a large molecule, usually interact differently with solvent molecules and with other intramolecular degrees of freedom, and therefore experience different frictions. A detailed study of such a situation is presented in Refs. 2(h) and 2(i).

An important point concerning experimental observations is the fact that the observable is not necessarily associated with the most stable product (or reactant) configurations, i.e., the point b (or a) of Fig. 1, but may correspond to the entire population on the product (or reactant) side of the ridge in Fig. 1. Thus, in the ligand–heme protein binding experiment the recombination product is observed spectroscopically, and the probe is sensitive to where the configuration is located on the multidimensional potential surface. In the case of CO binding to heme we may expect that gross changes in the optical spectrum, monitor crossings of the ridge that separates the reactant well (heme and ligand unbound) from the product well (heme and ligand bound). On the other hand, the dynamics of such activated processes is primarily controlled by the separatrix which is the boundary of the regions of attraction of the reactant and products wells. In cases where the observational separator (e.g., the ridge) differs substantially from the separatrix (Fig. 1), the probe employed will detect transient (nonexponential) behavior for the system. In this paper we provide a mathematical description of such a situation.

In Sec. II we describe our mathematical model and introduce our notation. We also show that under our simplifying assumption that the principal axes of the diffusion tensor and of the potential wells are parallel, only one parameter is needed to describe the two anisotropies. Section III provides the asymptotically long time solution for the reaction rate in this model and thus constitutes a generalization of Kramers' theory (in the diffusion limit) to nonisotropic situations. Section IV considers transients that, due to the anisotropy in the problem, can occur on experimentally important time scales. We end with a discussion of our results and some predictions.

II. FORMULATION

We consider the Smoluchowski system of equations corresponding to overdamped motion in the plane

$$\dot{\tilde{x}}_1 = -\frac{1}{m\gamma_1}\frac{\partial \tilde{V}}{\partial \tilde{x}_1} + \sqrt{\frac{2k_BT}{m\gamma_1}}\,\dot{w}_1,$$

$$\dot{\tilde{x}}_2 = -\frac{1}{m\gamma_2}\frac{\partial \tilde{V}}{\partial \tilde{x}_2} + \sqrt{\frac{2k_BT}{m\gamma_2}}\,\dot{w}_2, \tag{2.1}$$

where $\gamma_{1,2}$ are the friction coefficients (assumed large relative to all characteristic frequencies), k_B, T, and m denote the Boltzmann constant, the temperature, and the particle mass, respectively. Here $\dot{w}_1$ and $\dot{w}_2$ are independent standard Gaussian white noises. The potential $\tilde{V}(\tilde{x}_1,\tilde{x}_2)$ is assumed to have two minima located at $M_a = (\tilde{x}_{1a}, \tilde{x}_{2a})$ and $M_b = (\tilde{x}_{1b}, \tilde{x}_{2b})$ whose domains of attraction in the plane are denoted by $\tilde{\mathscr{D}}_a$ and $\tilde{\mathscr{D}}_b$, respectively. As shown below, these domains of attraction may be affected by the anisotropy. For an isotropic diffusion tensor they are determined by the potential alone and the separatrix (the common boundary of $\tilde{\mathscr{D}}_a$ and $\tilde{\mathscr{D}}_b$) is identical to the ridge in the potential surface. In the anisotropic case the ridge and the separatrix are not the same. We assume that there is a single saddle point $\tilde{S} = (\tilde{x}_{10},\tilde{x}_{20})$ of $\tilde{V}(\tilde{x}_1,\tilde{x}_2)$. The height of the potential barrier in $\tilde{\mathscr{D}}_i (i = a,b)$ is defined as $\Delta V_i = \tilde{V}(\tilde{x}_{10},\tilde{x}_{20}) - \tilde{V}(\tilde{x}_{1i},\tilde{x}_{2i})$. The Smoluchowski equation for the transition probability density $\rho(\tilde{x}_1,\tilde{x}_2,\tilde{t})$ of the process $[\tilde{x}_1(\tilde{t}),\tilde{x}_2(\tilde{t})]$ defined by Eq. (2.1) is

$$\frac{\partial \rho}{\partial \tilde{t}} = \frac{1}{m\gamma_1}\frac{\partial}{\partial \tilde{x}_1}(\tilde{V}_{\tilde{x}_1}\rho) + \frac{1}{m\gamma_2}\frac{\partial}{\partial \tilde{x}_2}(\tilde{V}_{\tilde{x}_2}\rho) + \frac{k_BT}{m}\left(\frac{1}{\gamma_1}\frac{\partial^2\rho}{\partial \tilde{x}_1^2} + \frac{1}{\gamma_2}\frac{\partial^2\rho}{\partial \tilde{x}_2^2}\right) \equiv \tilde{L}\rho, \tag{2.2}$$

whose stationary solution is

$$\rho = e^{-\tilde{V}/k_BT}. \tag{2.3}$$

Here $\tilde{V}_{\tilde{x}_i}$ denotes $\partial\tilde{V}/\partial\tilde{x}_i$. For simplicity of presentation, we have assumed that the principal axes of well $\tilde{\mathscr{D}}_a$, as well as the principal axes of the diffusion tensor, are parallel to the $\tilde{x}_1$, $\tilde{x}_2$ axes.

We nondimensionalize the problem by introducing the scalings:

$$x_1 = \frac{\tilde{x}_1}{L_1};\quad x_2 = \frac{\tilde{x}_2}{L_2};\quad t = \frac{\Delta V\tilde{t}}{mL_1^2\gamma_1};\quad V = \frac{\tilde{V}}{\Delta V} \tag{2.4}$$

and we introduce the two parameters ϵ and δ by

$$\epsilon = \frac{k_BT}{\Delta V},\quad \delta = \frac{\gamma_1}{\gamma_2}\frac{L_1^2}{L_2^2}. \tag{2.5}$$

Here the characteristic lengths L_1 and L_2 represent the widths of the reactant (a) well in the directions $\tilde{x}_1$ and $\tilde{x}_2$ respectively, and ΔV is its depth (barrier height).

We note that in dimensionless variables the barrier height is 1, and that the domains of attraction $\tilde{\mathscr{D}}_i$ $(i = a,b)$ of the stable equilibria M_a and M_b become $\mathscr{D}_i$ $(i = a,b)$. The scaled separatrix is denoted by Γ (see Fig. 1). The principal frequencies of vibration ω_1 and ω_2, at the bottom of the well $\mathscr{D}_a$, in dimensionless variables, are defined by

$$V_{x_1x_1}V_{x_2x_2} - V_{x_1x_2}^2|_{x_{1a},x_{2a}} = \omega_1^2\omega_2^2. \tag{2.6}$$

Finally, note that only one parameter δ is needed to characterize the anisotropy in the present simple model.

The deterministic dynamics [cf. Eq. (2.1) with $T=0$], in dimensionless variables, is written as

$$\dot{x}_1 = -V_{x_1}\,,$$
$$\dot{x}_2 = -\delta V_{x_2}\,. \tag{2.7}$$

For $\delta \ll 1$, we observe that there are two distinct time scales, t and δt. The relatively rapid dynamics in the x_1 direction, evolves on the time scale t, while the slow dynamics in the x_2 direction, evolves on the time scale δt. The separation of time scales will be employed to advantage in Sec. IV, where we analyze the long time transient behavior of the Fokker–Planck equation.

The dimensionless Fokker–Planck (Smoluchowski) equation for the probability density function ρ of the process $[x_1(t),x_2(t)]$ is

$$\rho_t = L\rho \equiv (V_{x_1}\rho)_{x_1} + \delta(V_{x_2}\rho)_{x_2} + \epsilon(\rho_{x_1x_1} + \delta\rho_{x_2x_2})\,. \tag{2.8}$$

Near the saddle point S, assumed to be located at (0,0) for simplicity, the potential V may be written locally as

$$V \sim \tfrac{1}{2}[Ax_1^2 + 2Bx_1x_2 + Cx_2^2] + \cdots\,. \tag{2.9}$$

We now describe the structure of the separatrix Γ, near $S=(0,0)$. The linearized deterministic dynamics has the form

$$\dot{x}_1 = -(Ax_1 + Bx_2)\,,$$
$$\dot{x}_2 = -\delta(Bx_1 + Cx_2)\,. \tag{2.10}$$

The eigenvalues of Eq. (2.10) are given by

$$\lambda_\pm = \frac{-(A+\delta C) \pm \sqrt{(A-\delta C)^2 + 4\delta B^2}}{2}, \tag{2.11}$$

with $\lambda_+ > 0$ and $\lambda_- < 0$, and the corresponding eigenvectors are given by

$$V_\pm = \begin{pmatrix} -B \\ A+\lambda_\pm \end{pmatrix}. \tag{2.12}$$

The saddle point condition is $AC < B^2$. We note that for small δ,

$$V_+ \sim \begin{pmatrix} -B \\ A \end{pmatrix}, \quad V_- \sim \begin{pmatrix} 1 \\ \delta B/A \end{pmatrix}, \quad \text{if } A>0, \tag{2.13a}$$

$$V_+ \sim \begin{pmatrix} 1 \\ \delta B/A \end{pmatrix}, \quad V_- \sim \begin{pmatrix} -B \\ A \end{pmatrix}, \quad \text{if } A<0, \tag{2.13b}$$

and

$$V_+ \begin{pmatrix} -B \\ \sqrt{\delta}|B| \end{pmatrix}, \quad V_- \sim \begin{pmatrix} B \\ \sqrt{\delta}|B| \end{pmatrix}, \quad \text{if } A=0. \tag{2.13c}$$

In all cases, the direction of the separatrix Γ at the saddle point S, is determined by the eigenvector V_-, associated with the negative eigenvalue λ_-. For $A>0$, we see that as $\delta \to 0$ (i.e., diffusion in the x_1 direction is much faster than in the x_2 direction), Γ approaches the x_1 axis, with an $O(\delta)$ angle between them. The fast diffusional motion (along x_1) is therefore nearly parallel to Γ, and crossing Γ essentially involves the slow diffusional component. In contrast, for $A<0$, the angle between Γ and x_1 is $O(1)$, and the crossing of Γ is dominated by the rapid diffusional motion. The intermediate case $A=0$, corresponds to an angle which is $O(\sqrt{\delta})$.

A trajectory $[x_1(t),x_2(t)]$ that starts at a point (x_1,x_2) in $\mathscr{D}_a$, hits Γ for the first time at a random time τ^*, at a point $x_1(\tau^*)=\xi_1$, $x_2(\tau^*)=\xi_2$. The scaled mean first passage time (MFPT) $\tau(x_1,x_2)$, from a point (x_1,x_2) in $\mathscr{D}_a$, to Γ, satisfies[8]

$$L^*\tau \equiv V_{x_1}\tau_{x_1} + \delta V_{x_2}\tau_{x_2} + \epsilon(\tau_{x_1x_1} + \delta\tau_{x_2x_2})$$
$$= -1 \quad \text{in } \mathscr{D}_a, \quad \tau = 0 \quad \text{on } \Gamma, \tag{2.14}$$

where L^* is adjoint to L. The MFPT is also referred to as the lifetime of the system in $\mathscr{D}_a$. The probability density of hitting points (ξ_1,ξ_2) on Γ, starting at a point (x_1,x_2) in $\mathscr{D}_a$, is Green's function $p(x_1,x_2,\xi_1,\xi_2)$ of the boundary value problem[8]

$$L^*u = 0 \quad \text{in } \mathscr{D}_a\,,$$
$$u = f \quad \text{on } \Gamma, \tag{2.15}$$

where f is an arbitrary smooth function, prescribed on Γ.

III. THE LIFETIME AND THE DISTRIBUTION OF HITTING POINTS

In this section we calculate the MFPT τ to reach Γ (the lifetime in $\mathscr{D}_a$), and the distribution p of hitting points on Γ. The MFPT determines the rate k at which the product well is populated at asymptotically long times, as the Kramers rate

$$k \sim \frac{1}{2\tau}, \tag{3.1}$$

where the factor 1/2 accounts for the fact that particles reaching Γ, are equally likely to cross Γ into the product well, or to return to the reactant well $\mathscr{D}_a$. (As discussed in Sec. I, this rate does not necessarily represent the time evolution of the system which is observed experimentally. These observations may correspond to shorter time transients, which will be studied in Sec. IV.) The rate k which we calculate, depends on the anisotropy parameter δ, and thus generalizes Kramers' two-dimensional formula.

A method for treating the singularly perturbed boundary value problem (2.14) for the MFPT τ, was introduced by Matkowsky and Schuss.[9] Employing this method in the form used in Ref. 10, we find that for $\epsilon \ll 1$ and $\delta = O(1)$, τ is given by

$$\tau \sim \frac{\pi\omega_r^B \Pi_{nr}\omega_{nr}^B}{\lambda_+ \Pi_j \omega_j^\omega}\, e^{1/\epsilon}, \tag{3.2}$$

where λ_+ [cf. Eq. (2.11)] is the positive eigenvalue of the linearized dynamics (2.10) about the saddle point. The result in the form was first obtained by Grote and Hynes.[2(h),2(i)] In the isotropic case ($\delta=1$), $\lambda_+ = (\omega_r^B)^2$ and Eq. (3.2) reduces to the dimensionless MFPT corresponding to the rate (1.1) according to $k = 1/2\tau$.

The extremely anisotropic limit $\delta \to 0$ yields

$$\tau \sim \frac{\pi A e^{1/\epsilon}}{\delta\sqrt{B^2 - AC}\,\omega_1\omega_2} \quad \text{if } A>0, \tag{3.3a}$$

$$\tau \sim \frac{\pi\sqrt{B^2 - AC}}{-A\omega_1\omega_2}\, e^{1/\epsilon} \quad \text{if } A<0, \tag{3.3b}$$

and

$$\tau \sim \frac{\pi e^{1/\epsilon}}{\sqrt{\delta \omega_1 \omega_2}}, \quad \text{if } A = 0. \tag{3.3c}$$

These three results are associated with the different relative directions of the rapid diffusional motion along x_1 and the separatrix Γ, near the saddle point S. For $A > 0$, the angle between the two directions was seen to be $O(\delta)$. In this case the process of crossing Γ is dominated by the slow component of the diffusional motion, so that $\tau = O(1/\delta)$. For $A < 0$, the angle is $O(1)$, as is τ, which is dominated by the rapid diffusional component. Finally, for $A = 0$, the angle is $O(\sqrt{\delta})$, and $\tau = O(1/\sqrt{\delta})$.

In this calculation, we first considered the limit $\epsilon \ll 1$ [leading to Eq. (3.2)], and then $\delta \ll 1$. If we reverse the order of taking the limits, i.e., we first consider $\delta \ll 1$ and then $\epsilon \ll 1$, the analysis proceeds differently. Nevertheless, it can be shown (Appendix) that the same result holds, i.e., the result is independent of the order of taking the limits. We also show in the Appendix that in the interesting case $A = 0$, the lifetime τ can be obtained, to leading order in δ, by solving a one-dimensional barrier crossing problem in the effective potential $V^{\text{eff}}(y)$ defined by

$$e^{-V^{\text{eff}}(y)/\epsilon} = \int_{-\infty}^{\infty} dx\, e^{-V(x,y)/\epsilon}, \tag{3.4}$$

where the starting point is $y = x_{2a}$ and where the barrier is located at the saddle point $y = x_{20}$. Thus in the extremely anisotropic limit the two-dimensional barrier crossing problem is reduced to a one-dimensional problem which is obtained by averaging over the fast coordinate. Note that since for $\epsilon \ll 1$, $V^{\text{eff}}(y)$ is essentially equal to $V[x(y), y]$ where $x(y)$ is that value of x for which $V[x(y), y]$ is a minimum for a given y, the reaction path y is exactly the minimum energy path leading from the bottom of the reactant well a, through the saddle point, to the product well b. This result should be contrasted with the picture of Agmon and Hopfield[6] in which the reaction is dominated by motion perpendicular to the reaction coordinate. As an example of the difference, consider a model where a double well potential surface is constructed from two shifted harmonic surfaces

$$V(x,y) = \min \begin{cases} \lambda_x x^2 + \lambda_y y^2 \\ \lambda_x (x-a)^2 + \lambda_y (y-b)^2 + \Delta E \end{cases}. \tag{3.5}$$

Defining $\delta = \lambda_x a^2 + \lambda_y b^2 + \Delta E$, we find that saddle point energy ΔV is given by

$$\Delta V = \frac{\delta^2}{4(\lambda_x a^2 + \lambda_y b^2)}. \tag{3.6}$$

This is also the activation energy associated with Eqs. (3.2) and (3.3). [Note however that the preexponential term will be different due to the discontinuity at the barrier, of the force associated with the model (3.5)]. On the other hand, the Agmon Hopfield result [based on the model (1.3)], in the fast diffusion limit [Eqs. (20), (35b) of Ref. 6(a)] is $k = \langle k(y) \rangle$ where $k(y)$ is the Kramers rate associated with the one-dimensional diffusional motion along the x axis for a given y and the average is taken over a thermal distribution in the y direction. The y dependent barrier for this motion is easily found to be

$$\Delta V(y) = \lambda_x \left(\frac{\delta - 2\lambda_y b y}{2\lambda_x a} \right)^2 + \lambda_y y^2. \tag{3.7}$$

Taking the average of $k(y) \sim e^{-\beta \Delta V(y)}$ over the thermal distribution $P(y) \sim e^{-\beta \lambda_y y^2}$ yields k in the form $k \sim e^{-\beta \Delta V^*}$, where

$$\Delta V^* = \frac{\delta^2}{2(2\lambda_x a^2 + \lambda_y b^2)} \tag{3.8}$$

which does not agree with Eq. (3.6). This is due to the fact that taking the fast diffusion limit in the y direction is incompatible with Eq. (1.3), at least in situations where the motion in the x direction is also diffusional.

This does not mean however that the behavior predicted by Agmon and Hopfield cannot be observed experimentally. Such effects can dominate in the transient regime before the asymptotically long time behavior sets in. This is discussed in the next section.

IV. TRANSIENT BEHAVIOR

The asymptotically long time behavior, governed by the MFPT, as described in Sec. III, may in some situations not represent the experimentally relevant behavior, as discussed in Sec. I. In this section we focus on the earlier transient behavior. We observe that for small δ, two time scales, fast and slow, govern this transient dynamics. On a relatively short time scale, local equilibrium is obtained in the x_1 direction within the reactant well. On a longer (but still transient) time scale, two processes occur: (i) transition over the ridge, which is dominated by the diffusion along the x_1 direction, and (ii) slow diffusion along the x_2 direction. On this (long, but not asymptotically long) time scale, the product region (for each x_2) is populated by what is effectively a continuous distribution of one-dimensional fluxes along x_1. The slow diffusivity along x_2 changes the relative weight of these fluxes, thus the average ridge crossing rate. This appears as a nonexponential relaxation behavior, which may, in some cases, be the dominant contribution to the observed dynamics. In order to describe this process mathematically, we employ the two time method,[12] to solve the dimensionless Fokker–Planck equation (2.8). Specifically, we assume the solution ρ is a function of both t and $t' = \delta t$, in the form

$$\rho(x_1,x_2,t,\delta,\epsilon) \sim \rho^0(x_1,x_2,t,t',\epsilon) + \delta \rho^1(x_1,x_2,t,t',\epsilon) + \cdots. \tag{4.1}$$

Therefore Eq. (2.8) becomes

$$\rho^0_t + \delta(\rho^0_{t'} + \rho^1_t) \sim (V_{x_1}\rho^0)_{x_1} + \epsilon \rho^0_{x_1 x_1} + \delta[(V_{x_2}\rho^0)_{x_2} + (V_{x_1}\rho^1)_{x_1} + \epsilon \rho^0_{x_2 x_2} + \epsilon \rho^1_{x_1 x_1}] + \cdots. \tag{4.2}$$

The leading term ρ^0 in the expansion (4.1) satisfies

$$L_0 \rho^0 \equiv (V_{x_1}\rho^0)_{x_1} + \epsilon \rho^0_{x_1 x_1} = \rho^0_t. \tag{4.3}$$

The general solution of Eq. (4.3), obtained by separation of variables, is

$$\rho^0 = \sum_{n=0}^{\infty} \rho^0_n(x_1,x_2) a_n(x_2,t') e^{-\lambda_n(x_2)t}, \tag{4.4}$$

where $\lambda_n(x_2)$ and $\rho^0_n(x_1,x_2)$ are the eigenvalues and eigen-

functions, respectively, of L_0 in Eq. (4.3), with x_2 held constant, and the coefficients $a_n(x_2,t')$ are as yet undetermined.

For $n=0$, we have $\lambda_0=0$ and $\rho_0^0=e^{-V(x_1,x_2)/\epsilon}$, while for $n=1$, $\lambda_1(x_2)$ is essentially Kramers' rate constant corresponding to the potential $V(x_1,x_2)$ for fixed x_2. The eigenvalue λ_1, as well as the corresponding eigenfunction ρ_1^0 were calculated in Ref. 13, as

$$\lambda_1(x_2)=\lambda_a(x_2)+\lambda_b(x_2) \tag{4.5}$$

with

$$\lambda_i(x_2)=\frac{\omega_i(x_2)\omega(x_2)}{2\pi}e^{-\Delta V^i(x_2)/\epsilon} \quad (i=a,b), \tag{4.6}$$

where $\Delta V^i(x_2)$ are the activation barriers along the x_1 direction for a fixed x_2, starting from the well i ($i=a,b$):

$$\Delta V^i(x_2)=V[x_1^c(x_2),x_2]-V[x_1^i(x_2),x_2)],$$

$x_1^i(x_2)$ ($i=a,b$) are the values of x_1 at which $V(x_1,x_2)$ achieves its local minimum in well i, for a given x_2, and $x_1^c(x_2)$ is the value of x_1 at which $V(x_1,x_2)$ achieves its local maximum for fixed x_2. The frequencies $\omega_i(x_2)$ and $\omega(x_2)$ are defined by $\omega_i^2(x_2)=V_{x_1x_1}[x_1^i(x_2),x_2]$ and $\omega^2(x_2)=-V_{x_1x_1}[x_1^c(x_2),x_2]$, and

$$\rho_1^0\sim e^{-V(x_1,x_2)/\epsilon}\left[\frac{\omega(x_2)}{\sqrt{2\pi}}\right.$$
$$\left.\times\int_0^{[x_1-x_1^c(x_2)]/\sqrt{\epsilon}}\exp\{-\omega^2(x_2)s^2/2\}ds+\frac{1}{2}\right]. \tag{4.7}$$

To find $a_0(x_2,t')$, we consider the next order equation

$$L_0\rho^1=-(V_{x_2}\rho^0)_{x_2}-\epsilon\rho^0_{x_2x_2}+\rho^0_{t'}. \tag{4.8}$$

The solvability condition for Eq. (4.8) is that the right-hand side of Eq. (4.8) must be orthogonal to 1, which is the solution of $L_0^*\phi=0$. Therefore,

$$\int_{-\infty}^{\infty}[(V_{x_2}\rho^0)_{x_2}+\epsilon\rho^0_{x_2x_2}-\rho^0_{t'}]dx_1=0. \tag{4.9}$$

Employing Eq. (4.4) in Eq. (4.8), we find that $a_0(x_2,t')$ satisfies

$$\epsilon a_{0,x_2x_2}-V^{\rm eff}_{x_2}(x_2)a_{0,x_2}-a_{0,t'}=0, \tag{4.10}$$

which is the backward Kolmogorov equation[8] for a one-dimensional diffusion in the effective potential (defined in Sec. III and the Appendix), on the slow time scale t'. Clearly $a_0(x,t')$ approaches a constant value asymptotically as $t=\to\infty$ at a rate which is dominated by the τ^0, which we calculated in Sec. III. The functions $a_n(x_2,t')$ are determined from solvability conditions for ρ^n, determined at $O(\delta^{n+1})$.

The population in the product well can now be calculated as

$$p(t)\sim\iint_{\text{product well}}[e^{-V(x_1,x_2)/\epsilon}a_0(x_2,\delta t)$$
$$+\rho_1^0(x_1,x_2)a_1(x_2,\delta t)e^{-\lambda_1(x_2,\epsilon)t}+\cdots]dx_1\,dx_2, \tag{4.11}$$

where a_0 satisfies Eq. (4.10), and λ_1 and ρ_1^0 are given in Eqs. (4.5) and (4.7), respectively. We note that since $\lambda_1(x_2,\epsilon)\to 0$, as $\epsilon\to 0$ while $\lambda_j(x_2,\epsilon)=O(1)$ for $j\geq 2$, after long enough time the evolution of $p(t)$ is dominated by $\lambda_1(x_2,\epsilon)$.

On the fast time scale t, the time evolution is dominated (for large enough t) by the second term in Eq. (4.11). (The first term describes the growth of the equilibrium population at asymptotically long times.) We observe that the evolution on this time scale is not necessarily a single exponential, but is rather described by a continuous distribution of rates $\lambda_1(x_2,\epsilon)$ which correspond to the continuous distribution of almost independent fluxes, depending on the point x_2, which cross the ridge in the x_1 direction. This distribution evolves on the slow time scale δt [via $a_1(x_2,\delta t)$] due to the slow diffusion along the x_2 axis. Only at much longer times (when all processes on the time scale t have relaxed) do we expect to obtain the asymptotic behavior described in the previous section.

V. CONCLUSIONS

We have extended Kramers' theory of chemical reactions in the diffusion limit, to cases where anisotropy in the multidimensional potential surface and/or in the diffusion tensor plays an essential role in determining the rate. Our result, given in Eq. (3.2), for the mean first passage time τ to reach the separatrix, which is related to the study state rate k by $k=1/2\tau$, explicitly depends on the anisotropy parameter: for $\delta\to 1$ it reduces to the well known multidimensional generalization of the Kramers' isotropic result, while for small δ it corresponds to a one-dimensional motion in an effective potential $V^{\rm eff}$, given by Eq. (3.11), along the direction of slow diffusion. As we saw, this small δ limit never leads to the large D limit of the model described by Eq. (1.3) [Eqs. (20) and (35b) of Ref. 6(a)]. That result was obtained as a Boltzmann average over the position dependent rates $k(x)$ of Eq. (1.3), while our result is obtained as the inverse of the MFPT to reach the barrier of the effective potential (3.11).

In addition, we note that while the usual treatment of Kramers' problem is an expansion in the small parameter $\epsilon=k_BT/\Delta V$, in the case of anisotropy there is the possibility of an additional small parameter δ. We have shown that the result for both ϵ and δ small, is independent of the order in which the limits are taken.

As a model for chemical reactions, the anisotropic model adds an important feature to the usual treatments of chemical reactions based on the diffusion equation. For reactions where the rearrangement leading from reactants to products involves motion of large and small atomic groups, each having different interactions with the solvent, the friction and diffusion tensors are expected to be strongly anisotropic. (Anisotropy in the structure of the wells appears because of the intrinsic shape of the molecular potential; we have seen that its consequences are essentially the same as that of the diffusion anisotropy.) This may lead, as noted previously, to a competition between the potentially rate determining steps of crossing the potential barrier, and diffusing in one particular direction. We have shown that in the very long time limit, the MFPT is given by the generalization (3.2) of the Kramers result. In this result the effect of anisotropy is primarily due to the geometry of the separatrix and of the reac-

tion path coordinate, near the saddle point. However, relatively long time transients may exist and sometimes dominate the experimentally relevant time scale. These transients may in turn be dominated by the slow diffusion process across a ridge of the potential, which is not necessarily the separatrix.

Such a picture has recently been used by Agmon and Hopfield[6] to analyze the kinetics of ligand attachment to a heme protein. However they analyzed such processes in terms of Eq. (1.3). This equation may be a valid description of a process in which diffusion along one coordinates is coupled to a nondiffusive chemical step (such as an electron transfer). For cases such as protein–ligand recombination in solution, where all relevant motions appear to be diffusive, Eq. (2.2) is the correct starting point. Both Eq. (1.3), and our treatment, lead to nonexponential time evolution in the transient regime as is frequently observed. This nonexponential behavior is associated with the "nonhomogeneous" nature of the process in this regime, where the observed kinetics is associated with a continuous distribution of nearly independent fluxes [cf. Eq. (4.11)]. A recent analysis by Agmon[14] of the low temperature behavior of the CO–myoglobin system gives support to this picture. We note that even though the Agmon analysis is done in terms of the Agmon Hopfield model, the essential ingredient—the superposition of independent fluxes—is the same as that seen in the transient regime of our present calculation.

Another feature of reactions in complex chemical systems, is the fact that when the dividing surface between reactant and product wells is defined operationally by an observation (e.g., a particular spectral shift may indicate that the system occupies only a specific part of configuration space), the dividing surface is not necessarily identical to the separatrix that separates reactants from products according to the stability of trajectories determined by the equations of motion. It is in such situations, where the mode of observation selects a transition surface not identical to the separatrix, that we expect the most pronounced nonexponential behavior. This also makes the interesting prediction that different kinetic behavior will be observed when different probes (e.g., different interrogating absorption wavelengths) are employed.

Finally we note that at higher temperatures the parameter ϵ is larger so that the MFPT τ becomes smaller and the time evolution becomes exponential sooner.

Kinetic processes involving real biomolecules are of course much more complicated than the simple model used in this paper. The numerous degrees of freedom and the multitude of possible intermediate configurations make a detailed theoretical analysis (short of full scale simulation) practically impossible. We believe however, that the simple model investigated contains enough of the essential physics of these processes, to be useful in achieving a qualitative understanding of the observed dynamics.

APPENDIX

Here we show that the results (3.3) can also be obtained by first taking the limit $\delta \ll 1$ in Eq. (2.14), and then taking the limit $\epsilon \ll 1$, i.e., reversing the order of the limiting procedures in Sec. III. We consider explicitly the case $A > 0$ only.

For $\delta \ll 1$, we expand τ as

$$\tau \sim \frac{\tau_0}{\delta} + \tau_1 + \cdots . \tag{A1}$$

The leading terms τ_0 and τ_1 in the expansion satisfy

$$\mathcal{L}_0^* \tau_0 \equiv \epsilon \tau_{0,x_1x_1} - V_{x_1}(x_1,x_2)\tau_{0,x_1} = 0 \tag{A2}$$

and

$$\mathcal{L}_0^* \tau_1 = -\epsilon \tau_{0,x_2x_2} + V_{x_2}(x_1,x_2)\tau_{0,x_1} - 1 , \tag{A3}$$

respectively. Equation (A2) implies that

$$\tau_{0,x_1} = e^{V(x_1,x_2)/\epsilon}\phi(x_2) , \tag{A4}$$

where $\phi(x_2)$ is an arbitrary function of x_2. For the solution of Eq. (A4) to be bounded, it must be independent of x_1, so that $\tau_0 = \tau_0(x_2)$ [recall that (x_1,x_2) is the starting point of the stochastic trajectory]. The solvability condition for Eq. (A3) is that the right-hand side of Eq. (A3) must be orthogonal to all solutions f of

$$\mathcal{L}_0 f \equiv \epsilon f_{x_1x_1} + (V_{x_1} f)_{x_1} = 0 , \tag{A5}$$

where the operator $\mathcal{L}_0$ is adjoint to the operator $\mathcal{L}_0^*$ defined in Eq. (A2). Therefore

$$\int e^{-V(x_1,x_2)/\epsilon}[-\epsilon \tau_{0,x_2x_2} + V_{x_2}(x_1,x_2)\tau_{0,x_2} - 1]dx_1 = 0, \tag{A6}$$

so that $\tau_0(x_2)$ satisfies the averaged equation

$$\epsilon \tau_{0,x_2x_2} - V_{x_2}^{\text{eff}}(x_2)\tau_{0,x_2} = -1, \tag{A7}$$

where V^{eff} is an effective potential, defined by

$$V_{x_2}^{\text{eff}}(x_2) = \frac{\int_{-\infty}^{\infty} e^{-V(x_1,x_2)/\epsilon} V_{x_2}(x_1,x_2)dx_1}{\int_{-\infty}^{\infty} e^{-V(x_1,x_2)/\epsilon} dx_1} \tag{A8a}$$

or

$$\int_{-\infty}^{\infty} e^{-V(x_1,x_2)/\epsilon}\, dx_1 = e^{-V^{\text{eff}}(x_2)/\epsilon}. \tag{A8b}$$

A sketch of V^{eff} is given in Fig. 2. We solve Eq. (A7) with the boundary conditions

$$\tau_{0,x_2}(x_{2a}) = \tau_0(x_{20}) = 0 \tag{A9}$$

which represent reflection at the bottom of the effective well and absorption at its barrier, respectively. We note that the barrier for $V^{\text{eff}}(x_2)$ is located at the saddle point ξ_{20}. [This follows from the argument that leads to Eq. (A11) below.] The exact solution of Eqs. (A7) and (A9) is given by

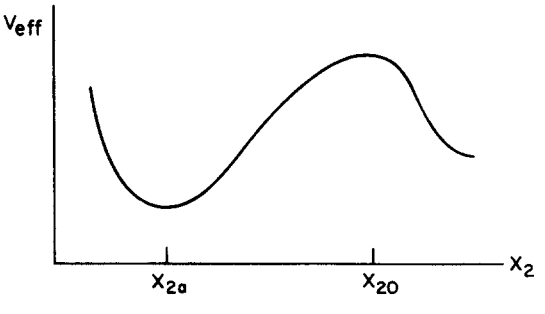

FIG. 2. A sketch of the effective potential [cf. Eq. (3.11)].

$$\tau_0(x_{2a}) = \frac{1}{\epsilon}\int_{x_{2a}}^{x_{20}} dz\, e^{V^{\text{eff}}(z)/\epsilon}\int_{z}^{x_{20}} dy\, e^{V^{\text{eff}}(y)/\epsilon}. \quad \text{(A10)}$$

Next we evaluate the integral $\int_{-\infty}^{\infty} dx\, e^{-V(x,y)/\epsilon}$ defining $V^{\text{eff}}(y)$ by the Laplace method[11] for each fixed y. The main contribution comes from the point $x_1 = x_1(y)$ where $V(x_1, y)$ has a minimum, namely,

$$V_{x_1}(x_1, y) = 0. \quad \text{(A11)}$$

Hence

$$\tau_0 \sim \frac{1}{\epsilon}\int_{x_{2a}}^{x_{20}}\int_{s}^{x_{20}} \frac{\sqrt{V_{x_1x_1}[x_1(y),y]}}{\sqrt{V_{x_1x_1}[x_1(z),z]}} \exp\left\{\frac{V[x_1(y),y] - V[x_1(z),z]}{\epsilon}\right\} dy\, dz$$

$$\sim \frac{\pi\sqrt{V_{x_1x_1}(x_{10},x_{20})}\, e^{1/\epsilon}}{\sqrt{(d^2/dy^2)V[x_1(y),y]|_{y=x_{20}}}\cdot\sqrt{(d^2/dy^2)V[x_1(y),y]|_{y=x_{2a}}}\cdot V_{x_1x_1}(x_{1a},x_{2a})}. \quad \text{(A12)}$$

To derive Eq. (A12) we recall that (i) contributions to the asymptotic form of the integral, from end points of integration, are one half the contributions from interior points, (ii) the barrier height in the scaled variables is 1, and finally (iii)

$$x_1(x_{2i}) = x_{1i} \quad (i = a,0). \quad \text{(A13)}$$

The second derivatives are calculated as

$$\frac{d^2}{dy}V[x_1(y),y] = V_{x_1x_1}x_1'^2 + 2V_{x_1x_2}x_1' + V_{x_2x_2}, \quad \text{(A14)}$$

where, by Eq. (A11),

$$x_1' \equiv \frac{dx_1(y)}{dy} = \frac{-V_{x_1x_2}}{V_{x_1x_1}}, \quad \text{(A15)}$$

so that

$$\frac{d^2}{dy^2}V[x_1(y),y] = \frac{-V_{x_1x_2}^2}{V_{x_1x_1}} + V_{x_2x_2}. \quad \text{(A16)}$$

Now, setting $y = x_{20}$, we obtain

$$\frac{d^2}{dy^2}V[x_1(y),y]|_{y=x_{20}} = \frac{AC - B^2}{A} \quad \text{(A17)}$$

and at $y = x_{2a}$ we obtain

$$\frac{d^2}{dy^2}V[x_1(y),y]|_{y=x_{2a}} = \frac{\omega_1^2\omega_2^2}{V_{x_1x_1}(x_{1a},x_{2a})}. \quad \text{(A18)}$$

Employing Eqs. (A17) and (A18) in Eq. (A12) we obtain Eq. (3.3a). The cases $A \leqslant 0$ can be handled in a similar manner.

[1] H. A. Kramers, Physica (Utrecht) **7**, 284 (1940).

[2] (a) H. C. Brinkman, Physics **22**, 149 (1956); (b) G. H. Vineyard, J. Phys. Chem. Solids **3**, 121 (1957); (c) R. Landauer and J. A. Swanson, Phys. Rev. **121**, 1668 (1961); (d) H. R. Glyde, Rev. Mod. Phys. **39**, 373 (1967); (e) J. S. Langer, Phys. Rev. Lett. **21**, 973 (1968); Ann. Phys. (N.Y.) **54**, 258 (1969); (f) Z. Schuss and B. J. Matkowsky, SIAM J. Appl. Math. **35**, 604 (1979); (g) Z. Schuss, *Theory and Application of Stochastic Differential Equations* (Wiley, New York, 1980); (h) R. F. Grote and J. T. Hynes, J. Chem. Phys. **74**, 4465 (1981); **75**, 2191 (1981); (i) G. van der Zwan and J. T. Hynes, *ibid.* **77**, 1295 (1982).

[3] (a) R. S. Larson and D. Koston, J. Chem. Phys. **77**, 5017 (1982); (b) R. S. Larson, Physica A **137**, 295 (1986).

[4] B. J. Matkowsky, A. Nitzan, and Z. Schuss, J. Chem. Phys. **88**, 4765 (1988).

[5] H. Frauenfelder and R. D. Young, Comments Mol. Cell. Biophys. **3**, 347 (1986).

[6] (a) N. Agmon and J. J. Hopfield, J.Chem. Phys. **78**, 6947 (1983); (b) **79**, 2042 (1983), and references therein.

[7] J. N. Onuchic, J. Chem. Phys. **86**, 3925 (1987); H. Sumi and R. A. Marcus, *ibid.* **84**, 4272 (1986); W. Nadler and R. A. Marcus **86**, 3906 (1987).

[8] Z. Schuss, *ibid.* Ref. 2(g).

[9] B. J. Matkowsky and Z. Schuss, SIAM J. Appl. Math. **33**, 356 (1977); (b) Z. Schuss and B. J. Matkowsky, *ibid.* **35**, 604 (1979); (c) B. J. Matkowsky and Z. Schuss, *ibid.* **42**, 822 (1982); (d) B. J. Matkowsky, Z. Schuss and C. Tier, *ibid.* **43**, 673 (1983); (e) B. J. Matkowsky and Z. Schuss, Phys. Lett. A **95**, 213 (1983).

[10] M. M. Dygas, B. J. Matkowsky, and Z. Schuss, SIAM J. Appl. Math. **46**, 265 (1986).

[11] C. M. Bender and S. M. Orszag, *Advanced Mathematical Methods for Scientists and Engineers* (McGraw–Hill, New York, 1978).

[12] J. Kevorkian and J. D. Cole, *Perturbation Methods in Applied Mathematics* (Springer, New York, 1981).

[13] B. J. Matkowsky and Z. Schuss, SIAM J. Appl. Math. **40**, 242 (1981).

[14] N. Agmon, Biochemistry **27**, 3507 (1988).